

See discussions, stats, and author profiles for this publication at: <https://www.researchgate.net/publication/265057194>

Structure and Properties of Nitrogen–Rich 1,4–Dicyanotetrazine, C₄N₆: A Comparative Study with Related Tetracyano Electron Acceptors

ARTICLE in THE JOURNAL OF ORGANIC CHEMISTRY · AUGUST 2014

Impact Factor: 4.72 · DOI: 10.1021/jo5014004 · Source: PubMed

READS

60

10 AUTHORS, INCLUDING:



Marçal Capdevila-Cortada

ICIQ Institute of Chemical Research of Catalonia

17 PUBLICATIONS 64 CITATIONS

[SEE PROFILE](#)



Saul H Lapidus

Argonne National Laboratory

32 PUBLICATIONS 226 CITATIONS

[SEE PROFILE](#)



Juan J. Novoa

University of Barcelona

276 PUBLICATIONS 5,487 CITATIONS

[SEE PROFILE](#)



Atta M. Arif

University of Utah

451 PUBLICATIONS 11,315 CITATIONS

[SEE PROFILE](#)

Structure and Properties of Nitrogen-Rich 1,4-Dicyanotetrazine, C₄N₆: A Comparative Study with Related Tetracyano Electron Acceptors

Hoa-Lan Vo,[†] Jordan L. Arthur,[†] Marçal Capdevila-Cortada,[‡] Saul H. Lapidus,^{§,||} Peter W. Stephens,[§] Juan J. Novoa,^{*,‡} Atta M. Arif,[†] Ramneet K. Nagi,[†] Michael H. Bartl,[†] and Joel S. Miller^{*,†}

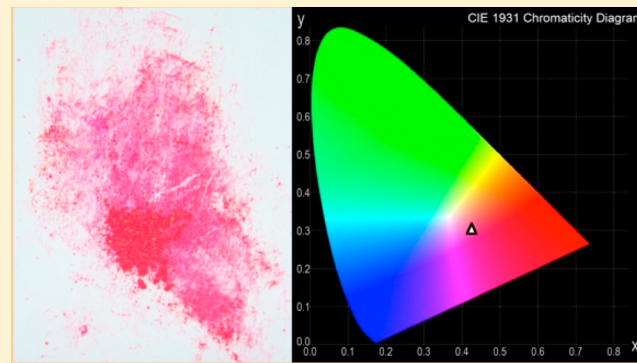
[†]Department of Chemistry, University of Utah, 315 South 1400 East, Room 2020, Salt Lake City, Utah 84112-0850, United States

[‡]Departament de Química Física and IQTCUB, Facultat de Química, Universitat de Barcelona, Av. Diagonal 645, 08028 Barcelona, Spain

[§]Department of Physics and Astronomy, Stony Brook University, Stony Brook, New York 11794, United States

S Supporting Information

ABSTRACT: The crystal structure, redox electrochemical stability, and reaction chemistry of 1,4-dicyanotetrazine (DCNT) has been experimentally characterized. These experimental results were rationalized by the results of theoretical calculations of the electronic structure, spin and charge distributions, electronic absorption spectra, and electron affinity and compared with the results for related the tetracyano electron acceptors tetracyanoethylene (TCNE), 7,7,8,8-tetracyano-*p*-quinodimethane (TCNQ), and 2,3,5,6-tetracyanopyrazine (TCNP). DCNT is made from the dehydration of 1,2,4,5-tetrazine-3,6-dicarboxamide, and because of the unusual deep-magenta color of the dicarboxamide in the solid state, its hydrogen-bonded layered structure, electronic structure, and electronic absorption spectra were determined. The magenta color is attributed to its absorptions at 532 nm (18 800 cm⁻¹), and this corresponds to normalized chromaticity coordinates of $x = 0.42$ and $y = 0.31$ in the pink/red/orange part of the 1931 CIE chromaticity diagram. In contrast with previous reports, DCNT exhibits an irreversible one-electron reduction at -0.09 V vs SCE (MeCN), and reduced forms of DCNT have yet to be isolated and characterized. In addition, the reactions of DCNT with V(CO)₆, Fe^{II}(C₅Me₅)₂, and I⁻ are discussed.



INTRODUCTION

The area of organic-based magnets is a growing contemporary area of materials chemistry.^{1,2} [Fe^{III}(C₅Me₅)₂]⁺[TCNE]^{•-} (TCNE = tetracyanoethylene), the first organic-based magnet, ferromagnetically orders at $T_c = 4.8$ K.^{3,4} The reaction of TCNE with either V(C₆H₆)₂⁵ or V⁰(CO)₆⁶ led to the first room-temperature organic-based magnet, V(TCNE)_x·zCH₂Cl₂ ($x \approx 2$; $z \approx 1/2$), with $T_c \approx 400$ K.⁵ Substitution of TCNE with 7,7,8,8-tetracyano-*p*-quinodimethane (TCNQ),⁷ 2,3,5,6-tetracyanopyrazine (TCNP),⁸ 2,3,5,6-tetracyanobenzene (TCNB),⁹ or *trans*-dicyanoperfluorostilbene¹⁰ led to magnets with reduced ordering temperatures.

With the goal of targeting new acceptors in which the radical anion stabilizes the magnetic ordering and can lead to the oxidation of V⁰(CO)₆, 1,4-dicyanotetrazine (DCNT) was identified as a possible candidate.¹¹ DCNT was reported to undergo a reversible one-electron reduction at 0.09 vs SCE in MeCN,¹² and hence, it is more difficult to reduce than TCNE [$E_{1/2}^{\circ} = 0.14$ V vs SCE (CH₂Cl₂)], TCNQ ($E_{1/2}^{\circ} = 0.17$ V), but easier than TCNP ($E_{1/2}^{\circ} = -0.31$ V).¹³ While these acceptors exhibit reversible one-electron reductions, none are sufficient to oxidize V(CO)₆ [$E^{+/0} = +0.88$ V vs SCE (CH₂Cl₂)].¹⁴ Nonetheless, as occurs for TCNE, TCNQ, TCNB, and TCNP, a

reaction with V⁰(CO)₆ via eq 1 is expected. We also targeted the reactions of 1,3,5-tricyanotriazine¹⁵ and 1,3,5-tricyanobenzene¹⁶ with V(CO)₆; however, they do not exhibit reversible one-electron reductions and upon reduction formed the diamagnetic σ dimers [C₁₂N₁₂]²⁻ and [C₁₂H₆N₆]²⁻, respectively;¹⁷ hence, the reaction with V⁰(CO)₆ did not form a magnetically ordered material.

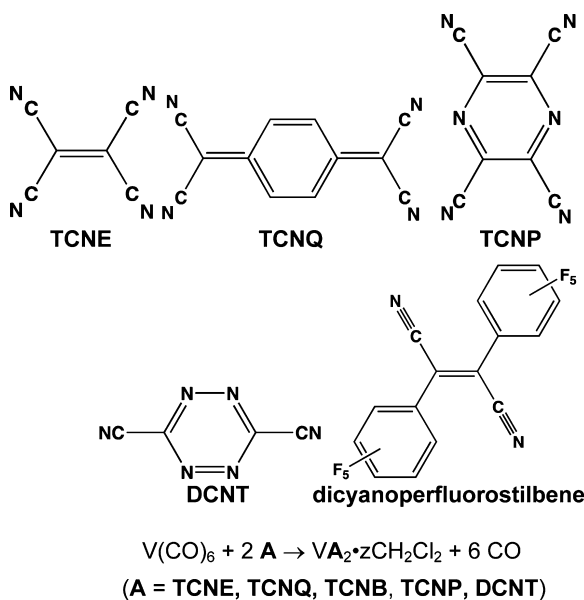
The reaction shown in eq 1 should form a compound in which μ -[DCNT]^{•-} bridges two V^{II} sites. This bridging is reduced with respect to [TCNE]^{•-}, [TCNQ]^{•-}, [TCNP]^{•-}, and [TCNB]^{•-}, as they can bond up to four V^{II} centers, and this may attenuate the spin coupling, which may lead to a reduced ordering temperature. Nonetheless, μ -[chloranil]^{•-} stabilizes the magnetic ordering in [Mn^{III}TPP][chloranil] (H₂TPP = *meso*-tetraphenylporphyrin) ($T_c = 13$ K).¹⁸ Furthermore, for example, the reaction of V(CO)₆ and *trans*-dicyanoperfluorostilbene forms a magnetically ordered material ($T_c = 205$ K).¹⁰

In addition to the interest in the identification of new organic-based magnets, there is growing interest in high-energy-density nitrogen-rich compounds with N:C ratios exceeding 1,

Received: June 23, 2014

Published: August 26, 2014





which also typically lack hydrogen,^{17,19} of which DCNT (N:C = 1.5) is an example.

Herein we report the crystal structure of DCNT, revisit its electrochemistry, explore its reduction, and experimentally and theoretically characterize it and its reduced species, $[\text{DCNT}]^{*-}$ with respect to the related tetracyano electron acceptors TCNE, TCNE^- , and TCNP as well as their potential use in electron transfer solids exhibiting properties of technological interest. In addition, the reactions of DCNT with $\text{V}(\text{CO})_6$, $\text{Fe}^{\text{II}}(\text{C}_5\text{Me}_5)_2$, and I^- are discussed.

RESULTS AND DISCUSSION

1. Synthesis and Crystallographic Characterization. DCNT was prepared by the steps outlined in Scheme 1, and the synthesis of magenta-colored 1,2,4,5-tetrazine-3,6-dicarboxamide (F) gave moderate to good yields. However, dehydration of F with phosphorus pentoxide only afforded DCNT in low yields. This can be attributed to phosphoric acid contamination during the sublimation process, which required a second purification. With nitrile groups at the 1 and 4 positions, DCNT has two coordinating sites for bonding to metal centers.

The tetrazine core of DCNT has a low-lying π^* MO, due to the presence of electronegative nitrogens, allowing for the facile formation of radical anions.²⁰ In addition, because of a reported reversible one-electron reduction at 0.09 V vs SCE,¹² it has the

potential to stabilize magnetically ordered organic-based magnets. While the key focus of this work was DCNT, diamide F was also isolated, and because of its unusual magenta color as a solid, its electronic absorption spectra as well as structure and MO diagram were studied. As a result of the poor solubility of F, except in DMSO and DMF, and the presence of several hydrogen-bond donors and acceptors, F is expected to have extensive hydrogen bonding in the solid state.

The geometry and electronic structure of DCNT were determined. The crystallographic parameters associated with the single-crystal X-ray structure of DCNT are reported in Table 1. DCNT is planar, exhibiting D_{2h} symmetry (Figure 1), with C–C, C–N, and N–N distances of 1.447(2), 1.3392(11), and 1.3232(16) Å, respectively. These are indicative of an expected aromatic behavior. DCNT packs in a herringbone motif (Figure 2) similar to that observed for benzene and aromatic fused-ring systems that do not have functional groups capable of forming hydrogen bonds, as the packing is driven by N···N and CN···NC van der Waals–dispersion interactions.²¹

The structure of F was determined from high-resolution X-ray powder patterns (Figure 3) by simulated annealing. The alternative model of nonaromatic E is excluded because refinements allowing two different C–N bond lengths converged to essentially equal values. Compound F is nearly planar with a *trans* regiochemistry (Figure 4). The carboxamide group is rotated 15° from the tetrazine ring in order to optimize hydrogen bonding. The ring C–N and N(sp²)···N(sp²) distances are 1.342(5) and 1.302(3) Å, while the carboxamide C–N, C–C, and C–O distances are 1.313(5), 1.504(7), and 1.319(4) Å, respectively. The packing of F differs substantially from that of DCNT, reflecting the presence of the two –CONH₂ groups that can exhibit strong hydrogen bonding via the hydrogen-bond donor (N–H) and a strong hydrogen-bond acceptor (the carbonyl O). The molecules form eight-membered rings of N–H···O=C hydrogen bonds (N–O distances of 2.84 and 2.91 Å) at both sides of each molecule, resulting in the formation of planes (Figure 4).²² These planes stack on top of each other via π – π -type van der Waals interactions.²³

2. Electronic Structure of $[\text{DCNT}]^{*-}$ and Comparison with $[\text{TCNE}]^{*-}$, $[\text{TCNQ}]^{*-}$, and $[\text{TCNP}]^{*-}$. With the above structure, MO calculations were carried out at the B3LYP/6-31+G(d) level for neutral DCNT and its reduced monoanion, $[\text{DCNT}]^{*-}$, to understand their electronic structures and for comparison with the electronic structures of $[\text{TCNE}]^{*-}$,^{24–26} $[\text{TCNQ}]^{*-}$,^{27,28} and $[\text{TCNP}]^{*-}$.²⁹ The MO diagram for neutral D_{2h} DCNT is presented in Figure 5a. The HOMO has a σ -antibonding nature, and the π -antibonding

Scheme 1. Synthetic Route to 1,4-Dicyanotetrazine (DCNT)

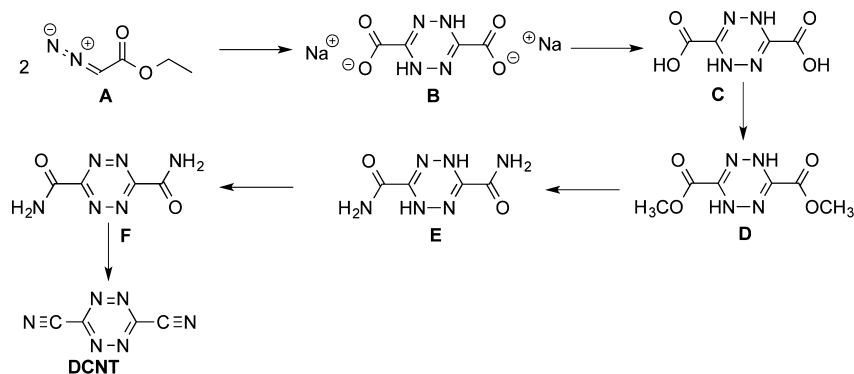


Table 1. Crystal Structure Refinement Data for DCNT and 1,2,4,5-Tetrazine-3,6-dicarboxamide (F)

	DCNT	F
empirical formula	C ₄ N ₆	C ₄ H ₄ N ₆ O ₂
formula weight	132.10	168.132
temperature (K)	150(1)	295
wavelength (Å)	0.71073	0.69998
crystal system	orthorhombic	monoclinic
space group	Cmca	P2 ₁ /c
<i>a</i> (Å)	6.6745(5)	9.1187(3)
<i>b</i> (Å)	9.0337(5)	5.0626(2)
<i>c</i> (Å)	9.4283(6)	6.6952(3)
β (deg)	90	88.492(3)
<i>V</i> (Å ³)	568.48(6)	308.97(2)
<i>Z</i>	4	2
calcd density (Mg/m ³)	1.543	1.807
absorption coefficient (mm ⁻¹)	0.115	0.095
final <i>R</i> indices [<i>I</i> > 2σ(<i>I</i>)]	$R_1^a = 0.0326$, $wR_2^b = 0.0801$	
<i>R</i> indices (all data)	$R_1 = 0.0378$, $wR_2 = 0.0828$	
$R_{wp}^{d,e}$		0.0846
$R_{exp}^{e,f}$		0.0380
goodness of fit on F^2 ^c	1.101	
largest diff. peak/hole (e Å ⁻³)	0.137/-0.149	

^a $R_1 = \sum(|F_o| - |F_c|)/\sum|F_o|$. ^b $wR_2 = \{\sum[w(F_o^2 - F_c^2)^2]/[\sum(w(F_o^2)^2)]\}^{1/2}$. ^cGoodness of fit on $F^2 = \{\sum[w(F_o^2 - F_c^2)^2]/(n - p)\}^{1/2}$, where *n* is the number of reflections and *p* is the number of parameters refined. ^d $R_{wp} = \{\sum_i[w_i(y_i^{\text{calcd}} - y_i^{\text{obs}})^2]/\sum_i[w_i(y_i^{\text{obs}})^2]\}^{1/2}$. ^e y_i^{calcd} and y_i^{obs} are the calculated and observed intensities at the *i*th point in the profile, normalized to monitor intensity. The weight w_i is $1/\sigma^2$ from the counting statistics, with the same normalization factor. *N* is the number of points in the measured profile minus number of parameters. ^f $R_{exp} = \{N/\sum_i[w_i(y_i^{\text{obs}})^2]\}^{1/2}$.

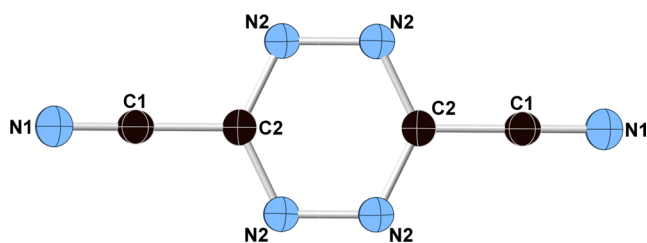


Figure 1. Atom labeling and thermal ellipsoid (50% probability) plot of DCNT: N1–C1 1.1390(19) Å, N2–N2#1 1.3232(16), N2–C2 1.3392(11) Å, C1–C2 1.447(2) Å, C2–N2#2 1.3392(11) Å, N2#1–N2–C2 115.96(7)°, N1–C1–C2 177.68(16)°, N2#2–C2–N2 128.08(13)°, N2#2–C2–C1 115.95(7)°, and N2–C2–C1 115.95(6)°.

LUMO has weak contributions from the two cyano groups. The character of these frontier MOs is at variance with respect to that reported for TCNE,^{54,25,26} TCNQ,^{27,28} and TCNP.²⁹ The results from the computations for [DCNT]^{•-} at the B3LYP level confirm that the SOMO corresponds to the LUMO of neutral DCNT (Figure 6).

As a consequence of this shape, the distributions of spin (Figure 7) and charge (Figure 8) of [DCNT]^{•-} have negligible contributions from the two CN groups. The spin density (ρ^s) is governed by the difference between the α and β electron densities (ρ^α and ρ^β , respectively): $\rho^s = \rho^\alpha - \rho^\beta = |\Psi(\alpha)|^2 - |\Psi(\beta)|^2$. When the α and β orbitals below the SOMOs have similar shapes and stabilities (i.e., when polarization effects are not important), $\rho^s \approx |\Phi_{\text{SOMO}}(\alpha)|^2$, that is, the square of the absolute value of the SOMO orbital.³⁰ However, the electron

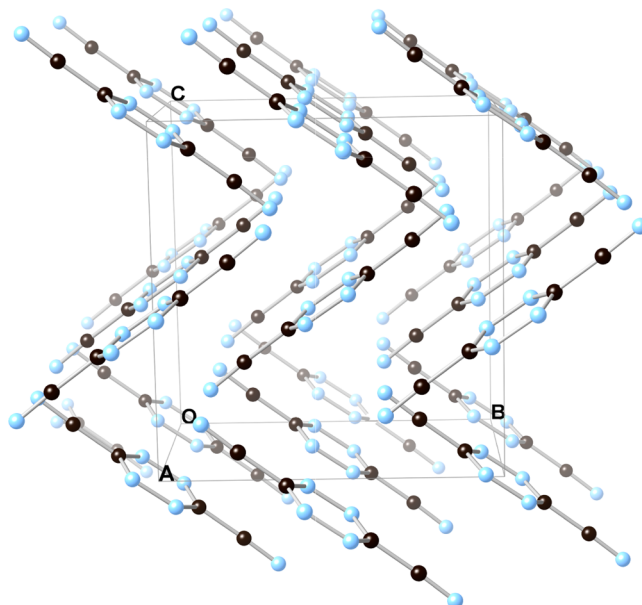


Figure 2. Interleaving herringbone packing motif of DCNT.

density, defined as $\rho = \rho^\alpha + \rho^\beta = |\Psi(\alpha)|^2 + |\Psi(\beta)|^2$, can be written as $\rho \approx \sum_i|\Phi_i(\alpha)|^2 + \sum_j|\Phi_j(\beta)|^2$, that is, the sum of the squares of the absolute values of the α and β orbitals. Hence, most of the spin and electron density distributions may be located on different atoms. This is the case in [DCNT]^{•-}, where the spin mostly resides over the six-membered-ring atoms, with 0.31 e⁻ (positive values indicate a net α spin) on each N atom and -0.12 e⁻ (net β spin) on the two C atoms of the ring (Table 2). The charge distribution is slightly different, as the ring N atoms have an extra -0.18 e⁻ compared with DCNT, the two C atoms of the ring get a small -0.04 e⁻, while the rest of the extra charge goes to the nitrile N atom. The negligible value of the SOMO in some of the regions receiving a relevant amount of the spin and net charge (the ring C atoms and the C and N atoms of the nitriles) reflects an important polarization of the spin density. The shape of the charge distribution in [DCNT]^{•-} is better appreciated from the molecular electrostatic potential (MEP) map (Figure 8) and a comparison with the MEP map for neutral DCNT (Figure 9). The MEP map visually describes the regions of charge localization over the molecule. For [DCNT]^{•-}, the most negative regions of the MEP map are located on the ring N atoms, where the spin also accumulates (Figure 7 and Table 3). In sharp contrast, the MEP maps for [TCNE]^{•-}, [TCNQ]^{•-}, and [TCNP]^{•-} (Figure 8) and the corresponding neutral species (Figure 9) reveal that the extra negative charge and the spin are mostly located on the nitriles (Table 3), in good agreement with previous ab initio studies on [TCNE]^{•-},²⁴ [TCNQ]^{•-},²⁸ and [TCNP]^{•-}.²⁹ The different behavior is attributed to the unusual form of the [DCNT]^{•-} SOMO. Consequently, the spin is less protected by Coulombic repulsion for [DCNT]^{•-}, and it has a greater tendency to either σ - or π -dimerize than [TCNE]^{•-}, [TCNQ]^{•-}, an [TCNP]^{•-}, which is in accord with the inability to isolate [DCNT]^{•-}.

The MEP maps also contain information on the electrostatic component of the interaction energy (strictly, they map the interaction energy between the molecule of interest and a 1+ charge at the given point, the 1+ charge placed at the same distance of the molecule). For most ionic crystals, the

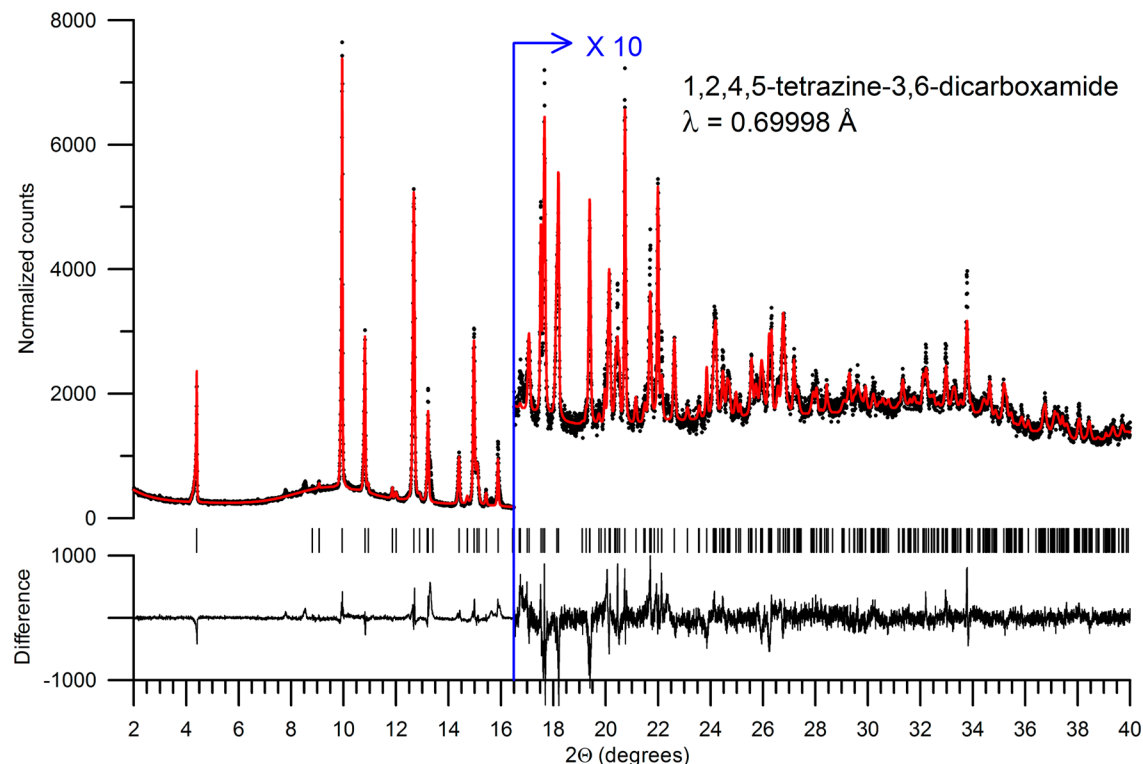


Figure 3. High-resolution synchrotron powder diffraction data (dots) and Rietveld fit of the data (line) for the structure of 1,2,4,5-tetrazine-3,6-dicarboxamide (**F**). The lower traces for each plot are the differences (measured – calculated) plotted on the same vertical scale.

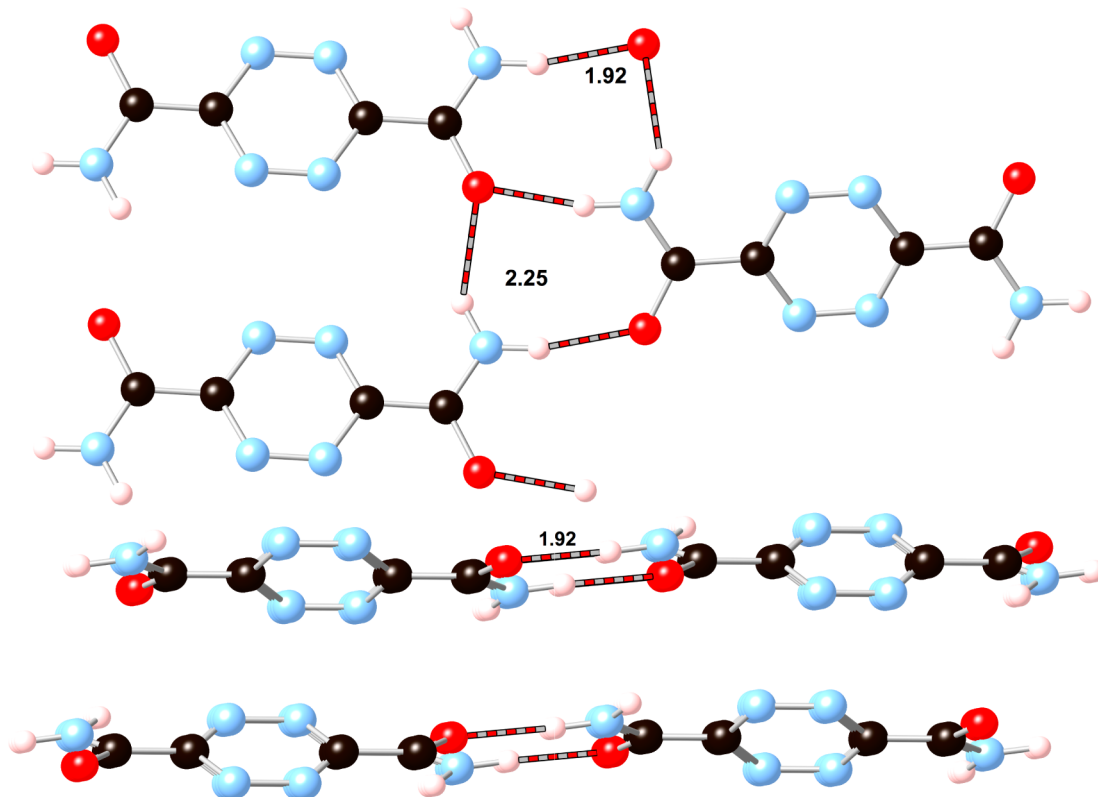


Figure 4. Top and side views of the structure of 1,2,4,5-tetrazine-3,6-dicarboxamide (**F**) and intralayer hydrogen bonding. The interlayer separation is 3.35 Å ($c/2$).

electrostatic interaction shown in the MEP map is the dominant energetic component. The similarity between the MEP map for $[\text{DCNT}]^{\bullet-}$ and those for $[\text{TCNQ}]^{\bullet-}$,

$[\text{TCNQ}]^{\bullet-}$, and $[\text{TCNP}]^{\bullet-}$ in Figure 8 is noteworthy and indicates that the packing of these radical anions is driven by the same energetic considerations. As in ionic salts, the

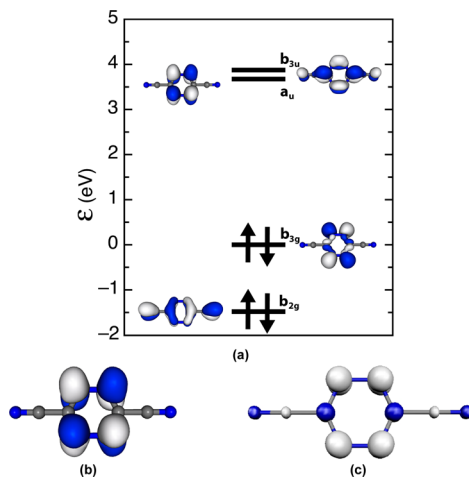


Figure 5. (a) MO diagram for D_{2h} DCNT. (b, c) Plots showing (b) the SOMO and (c) the computed spin density for $[DCNT]^{•-}$. The 0.03 au isosurface is shown for the SOMO, while the 0.005 au isosurface is shown for the spin density. Blue and white indicate regions of positive and negative values of the spin density, respectively. The four orbitals shown in (a) can also be classified according to their behavior with respect to the symmetry plane that contains the molecular plane: following a top-down ordering, these orbitals would be of π^* (as it has four CN nodes in the ring and two in the cyano groups), π^* , σ^* , and π^* symmetry, respectively.

dominant component of the interaction energy between all species is the electrostatic component that is graphically represented in the MEP maps. The similarity of their MEP maps indicates similar packing of these radical anions for the same cation (a trend that is not necessarily valid for other anions, whose shapes and/or electronic distributions are not similar³¹).

3. Electron Affinities of DCNT, TCNE, TCNQ, and TCNP in the Gas Phase and Solution. The difference between the total energies of DCNT and $[DCNT]^{•-}$ is the electron affinity (EA) of DCNT, and it was computed to be 2.9 eV in the gas phase and 4.5 eV in MeCN (obtained using the PCM continuous solvation model), as shown in Table 4, where the values are compared with those for TCNE, TCNQ, and TCNP. Previous studies have shown that it is possible to reproduce the

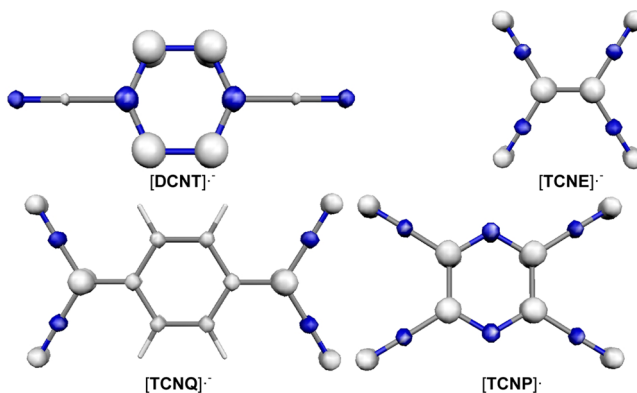


Figure 7. Computed spin distributions for $[DCNT]^{•-}$, $[TCNE]^{•-}$, $[TCNQ]^{•-}$, and $[TCNP]^{•-}$ at the 0.01 au isosurface. White indicates positive regions of spin density, where $\rho^\alpha > \rho^\beta$; blue indicates negative regions, where $\rho^\alpha < \rho^\beta$.

experimental EAs of a large number of molecules by accurate ab initio methods [e.g., CCSD(T), CASPT2] and, with slightly less accuracy, by density functional theory calculations.³² The computed EA values are positive, indicating that the anions are more stable than the parent neutral molecules.

The EAs computed herein at the B3LYP/6-31++G(d,p) level for TCNE and TCNQ are similar to the reported experimental values and also to the most accurate computational results [obtained at the CASPT2 and CCSD(T) levels], which also are close to the experimental values. Both B3LYP results are 0.5 eV smaller than the best computed values. The dispersion in the experimental results does not allow a more precise assessment of quality. This dispersion is probably due to the fact that some experiments measure vertical EAs and others diabatic EAs, among other factors. The B3LYP-computed value of the gas-phase EA of DCNT is 2.9 eV (Table 4), which is comparable to a previous estimate of 2.51 eV obtained using the semiempirical HAM/3 method.¹²

The computed EA values can also be compared with the closely related solution reduction half-wave potentials ($E_{1/2}^\circ$) for DCNT, TCNE, TCNQ, and TCNP (Table 4), which increase in the order $TCNP < DCNT < TCNE < TCNQ$. It should be noted that (a) the $E_{1/2}^\circ$ values are 1 order of magnitude smaller

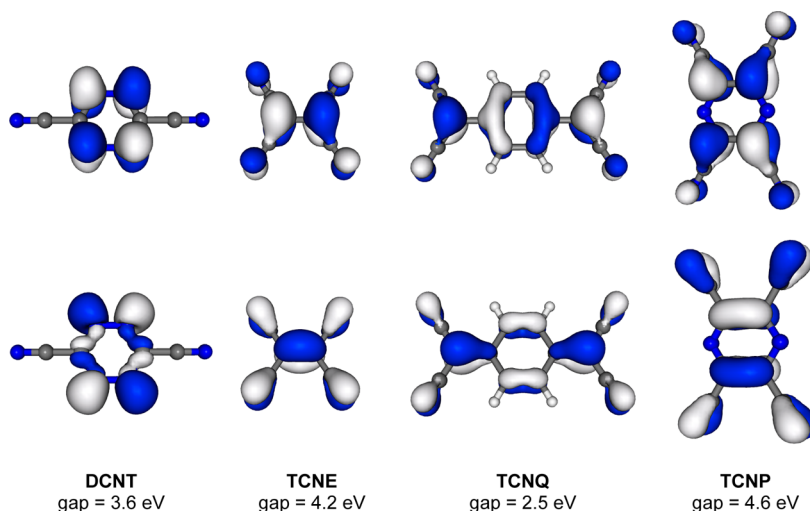


Figure 6. (top) LUMOs and (bottom) HOMOs of DCNT, TCNE, TCNQ, and TCNP (the 0.03 au isosurfaces are shown). Also shown are the HOMO–LUMO gaps computed at the B3LYP/6-31++G(d,p) level.

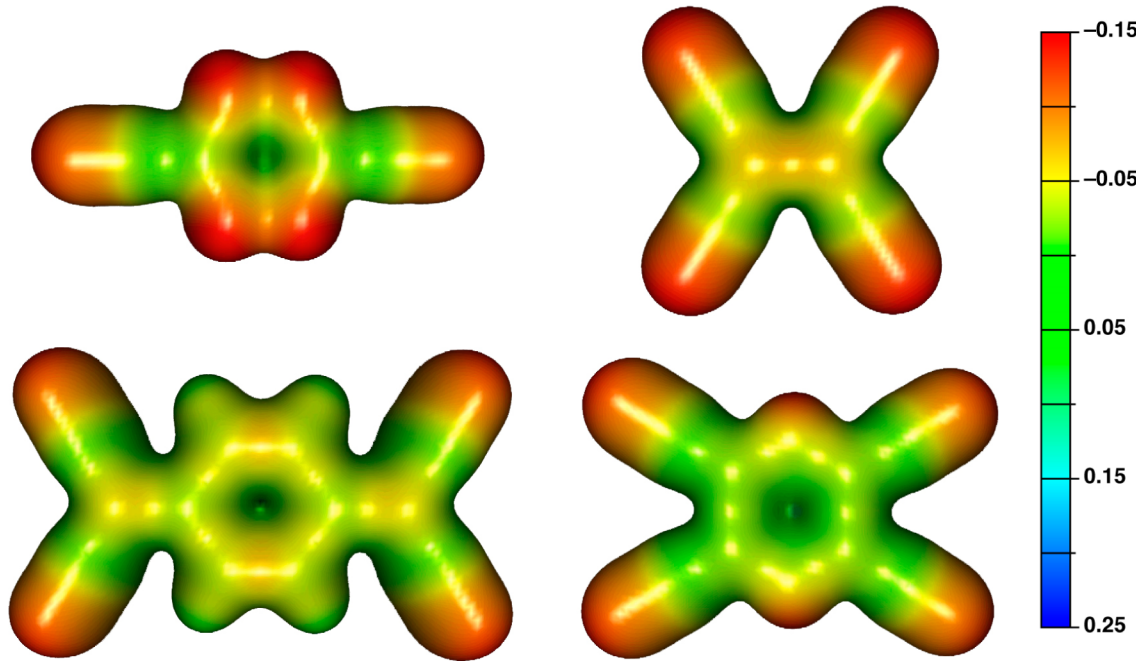


Figure 8. Molecular electrostatic potential (MEP) maps projected on the 0.03 au isosurfaces for $[DCNT]^{•-}$, $[TCNE]^{•-}$, $[TCNQ]^{•-}$, and $[TCNP]^{•-}$. Red indicates negative electrostatic potential (i.e., regions where the net charge is negative), while blue indicates regions where the electrostatic potential is positive. The scale at the right is the same as that used in Figure 9.

Table 2. Mulliken and NBO Atomic Charge Distributions (in Atomic Units) for D_{2h} DCNT and $[DCNT]^{•-}$ (Values in Parentheses Indicate the Variation with Respect to the DCNT Charge on the Same Atom) and the Mulliken Atomic Spin Densities for $[DCNT]^{•-}$ ^a

atom	DCNT		$[DCNT]^{•-}$		
	Mulliken charge population	NBO charge population	Mulliken charge population	NBO charge population	Mulliken spin population
C1 ^b	0.09	0.24	0.14 (+0.06)	0.31 (+0.07)	0.03
N1 ^b	-0.49	-0.20	-0.64 (-0.15)	-0.36 (-0.16)	-0.03
C2	0.44	0.26	0.39 (-0.05)	0.22 (-0.04)	-0.12
N2	-0.02	-0.15	-0.20 (-0.18)	-0.33 (-0.18)	0.31

^aOnly values for symmetry-unique atoms are given. See Figure 1 for the numbering convention. ^bNitrile atoms.

than the experimental EA values, a fact that reflects their different scales of reference as well as possible impacts of the solvent and other medium effects, and (b) the experimental $E_{1/2}^{\circ}$ values do not follow the relative ordering of the experimental EA values. The EAs computed using the PCM method do not reproduce the magnitude and relative ordering of the $E_{1/2}^{\circ}$ values in solution. These results suggest that the $E_{1/2}^{\circ}$ values are determined by more factors than the bare solvent effects and that a more detailed analysis is needed to understand the relationship between EA and $E_{1/2}^{\circ}$ in these compounds.³³

4. Electronic Absorption Spectra of DCNT, TCNE, TCNQ, TCNP, and F. The electronic absorption (UV-vis) spectrum of a 0.1 mM solution of orange-red DCNT in MeCN has a strong absorption at $45\ 000\ \text{cm}^{-1}$ ($\epsilon = 57\ 000\ \text{cm}^{-1}\ \text{M}^{-1}$) and weaker absorptions at $36\ 600\ \text{cm}^{-1}$ ($\epsilon = 17\ 400\ \text{cm}^{-1}\ \text{M}^{-1}$) and $20\ 400\ \text{cm}^{-1}$ ($\epsilon = 2500\ \text{cm}^{-1}\ \text{M}^{-1}$) (Figure 10 and Table 5). Its precursor, the air-stable bright orange-red colored compound 1,2,4,5-tetrazine-3,6-dicarboxamide (F) has very broad absorption bands at $\sim 38\ 800\ \text{cm}^{-1}$ ($\epsilon = 7500\ \text{cm}^{-1}\ \text{M}^{-1}$) and $19\ 200\ \text{cm}^{-1}$ ($\epsilon = 840\ \text{cm}^{-1}\ \text{M}^{-1}$) in DMSO. F exhibits a magenta color as a solid (dispersed in Nujol), and this is attributed to broad absorptions at $37\ 000$ and $18\ 600\ \text{cm}^{-1}$. The absorption band in

the visible region at $\sim 19\ 000\ \text{cm}^{-1}$ that is present in both compounds is typical of a tetrazine ring³⁵ and results in the observed color for F.

To more accurately determine the absorption of F in the visible region of the spectrum, the diffuse-reflectivity spectrum versus a BaSO_4 white standard was recorded and converted to an absorption spectrum (Figure 10). It has a broad absorption band peaking at a wavelength of about $18\ 800\ \text{cm}^{-1}$, giving rise to the magenta color of the powder.

To obtain a more quantitative description of the color of this compound, we determined its chromaticity coordinates.³⁶ This was done by combining the absorbance (transmission) properties of F with the color-matching functions of the 1931 CIE standard 2° observer.³⁷ The resulting chromaticity coordinates, $x = 0.42$ and $y = 0.31$, place the color in the pink/red/orange part of the 1931 CIE chromaticity diagram (Figure 11).

The interpretation of these spectra was aided by the MO diagrams for DCNT and F, shown in Figures 5 and 12, respectively. The electronic absorption spectra of DCNT and F were computed at the TD-DFT level using the B3LYP functional and the 6-31+G(d,p) basis set. The predicted spectrum for each molecule (Table 5 and Figure 13) reproduces the experimental

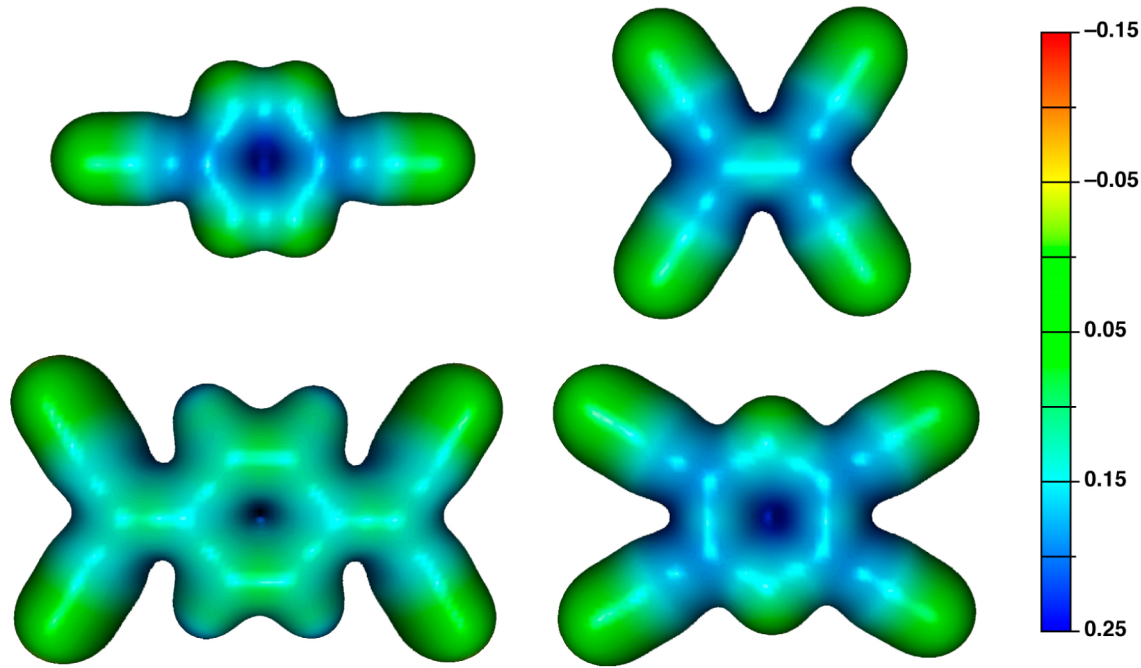


Figure 9. MEP maps projected on the 0.03 au isosurfaces for DCNT, TCNE, TCNQ, and TCNP. Red indicates negative electrostatic potential (i.e., regions where the net charge is negative), while blue indicate regions where the electrostatic potential is positive. The scale at the right is the same as that used in Figure 8.

Table 3. Sums of Mulliken Spin Densities (in Atomic Units) for $[DCNT]^{*-}$, $[TCNE]^{*-}$, $[TCNQ]^{*-}$, and $[TCNP]^{*-}$ Obtained at the B3LYP/6-31++G(d,p) Level; The Values Are Grouped as the Sums of the Spins on the Atoms in the Nitrile Groups (“total CN”) and the Spins on the Central Ring (“total backbone”)^a

	total CN	total backbone
$[DCNT]^{*-}$	0.00	1.00
$[TCNE]^{*-}$	0.25	0.75
$[TCNQ]^{*-}$	0.16	0.84
$[TCNP]^{*-}$	0.21	0.79

^aIn $[TCNQ]^{*-}$, the four hydrogens and the two carbons bonded to the central ring are considered as backbone atoms.

spectrum (Figure 10) very well. The UV-vis spectrum of DCNT in MeCN has three absorptions at positions and intensities that are in agreement with the TD-DFT results. The most intense absorption, at $45\,000\text{ cm}^{-1}$, is predicted to be at $41\,200\text{ cm}^{-1}$ and is assigned to the HOMO-1 \rightarrow LUMO+1 ($\pi^* \rightarrow \pi^*$) transition. The two weaker absorptions at $36\,600$ and $20\,400\text{ cm}^{-1}$ arise from the HOMO-1 \rightarrow LUMO ($\pi^* \rightarrow \pi^*$) and HOMO \rightarrow LUMO ($\sigma^* \rightarrow \pi^*$) transitions, respectively (Table 5 and Figure 5).

Table 4. Computed Electron Affinities (EAs)^a of DCNT, TCNE, TCNQ, and TCNP in the Gas Phase and in MeCN and CH_2Cl_2 Solution, Together with Experimental Values of $E_{1/2}^o$

acceptor	computed gas-phase EA (eV)	observed gas-phase EA (eV)	computed EA in MeCN (eV)	computed EA in CH_2Cl_2 (eV)	$E_{1/2}^o$ in MeCN (V vs SCE)
TCNP	3.2^b		4.4^b	4.3^b	-0.31^{13}
DCNT	$2.9^b, 2.51^{c,12}$		4.5^b	4.4^b	-0.09^b
TCNE	$3.5^b, 2.94^{d,25}$	$2.88^{e,34}, 2.9^{,60}, 3.17^{61}$	5.0^b	4.9^b	0.14^{13}
TCNQ	$3.7^b, 3.22^{d,28}$	$2.83^{e,34}, 2.8^{,62}, 2.84^{,60}, 4.23^{63}$	4.9^b	4.8^b	0.17^{13}

^aThe EA values were computed as $EA = E(\text{neutral}) - E(\text{anion})$; each energy was obtained at the B3LYP/6-31++G(d,p) level, using the PCM approach to model the solution environments. ^bThis work. ^cObtained using the semiempirical HAM/3 method. ^dObtained by CCSD(T) calculations. ^eObtained using the magnetron method.

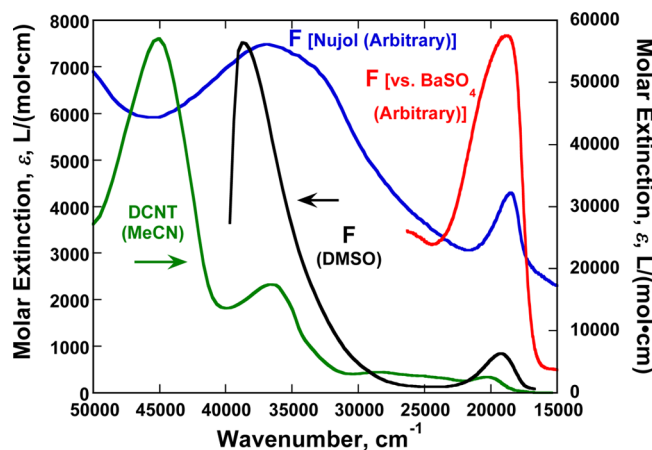


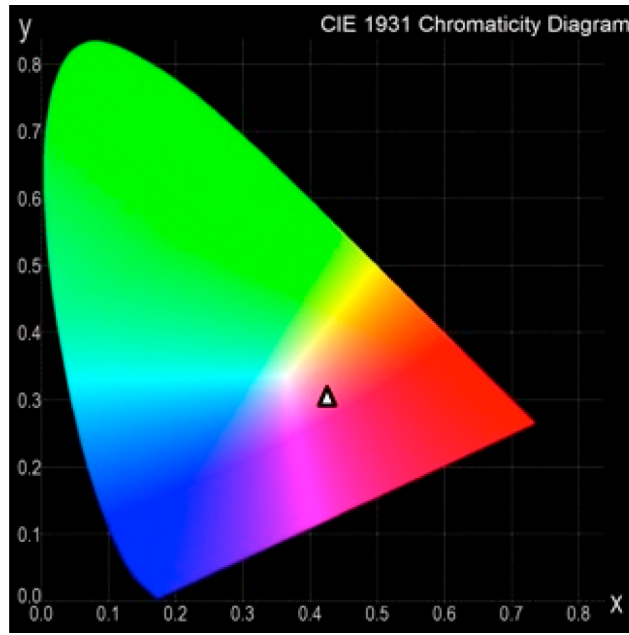
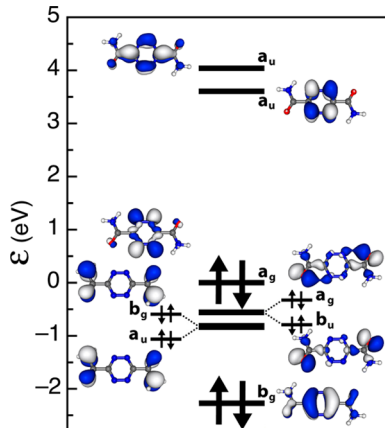
Figure 10. UV-vis spectra of DCNT in MeCN (green) and 1,2,4,5-tetrazine-3,6-dicarboxamide (F) in DMSO (black), in Nujol (blue), and vs $BaSO_4$ (red).

The UV-vis spectrum of the bright-magenta precursor F has two absorption bands in DMSO solution (or dispersed in Nujol): a stronger absorption at $38\,800\text{ cm}^{-1}$, which is very

Table 5. Energies (in cm^{-1}) of the Lowest-Energy Non-negligible Electronic Transitions in DCNT, F, TCNE, TCNQ, and TCNP^a

DCNT		F		TCNE		TCNQ		TCNP	
calcd	exptl	calcd	exptl ^b	calcd	exptl ^c	calcd	exptl ^d	calcd	exptl ^e
18200 (0.005) H → L	20400 (2500)	17770 (0.004) H → L		34500 (0.41) H → L	38300 (17000)	23800 (1.06) H → L	25400 (s)	33900 (0.13) H → L+1	33700 (7900)
—	—	29500 (0.19) H-3 → L	19200 (840)	42300 (0.14) H-2 → L		39700 (0.08) H-5 → L	43900 (w)	35900 (0.28) H → L	39500 (12100)
—	—	34400 (0.029) H-3 → L+1						43500 (0.68) H-2 → L	47000 (29800)
36650 (0.025) H-1 → L	36600 (17400)	42500 (0.032) H-5 → L	38800 (7500)						
41200 (0.49)	48000 (57000)	47500 (0.46) H-1 → L+1							

^aThe two orbitals involved for each transition are indicated (H = HOMO; L = LUMO), as is its predicted relative intensity. For the computed values, the numbers in parentheses are relative intensities. For the observed values, the numbers in parentheses are molar extinction coefficients (ϵ , in $\text{cm}^{-1} \text{M}^{-1}$) in MeCN; when no values are available, the bands are classified as strong (s) or weak (w). ^bIn DMSO.

**Figure 11.** CIE chromaticity diagram for F. The resulting chromaticity coordinates, $x = 0.42$ and $y = 0.31$, are indicated by the white triangle.**Figure 12.** MO diagram showing the shapes and relative energies (ϵ) of the LUMO+1 to HOMO-5 orbitals (top to bottom) for F. The near degeneracy of the HOMO-1 and HOMO-2 orbitals as well as the HOMO-3 and HOMO-4 orbitals should be noted. The four lowest doubly occupied orbitals are nearly degenerate on this energy scale. When the scale is multiplied by a factor of 10 (left and right insets) their apparent degeneracy disappears. The symmetries of all of the orbitals (in the C_{2h} point group for the fully optimized geometry) are also indicated. They could also be classified according to their behavior with respect to the symmetry plane that contains the molecular plane: following a top-down ordering, these orbitals would be of symmetry π^* , π^* , σ^* , σ (nonbonding), π (nonbonding), σ (nonbonding), π (nonbonding), and π^* , respectively.

broad in the Nujol spectrum, and a weaker absorption in the visible region at $19\ 200\ \text{cm}^{-1}$. The latter is also present in DCNT and is typical of a tetrazine ring.³⁵ The B3LYP calculations indicate that the most intense band for DCNT corresponds to the HOMO-1 \rightarrow LUMO ($\pi^* \rightarrow \pi^*$) transition, while in F it is associated with a HOMO-3 \rightarrow LUMO+1 [σ (nonbonding) $\rightarrow \pi^*$] transition (Table 5 and Figure 5). Additionally, the computed spectrum of F has a very intense absorption at $\sim 50\ 000\ \text{cm}^{-1}$ assigned to the HOMO-5 \rightarrow LUMO+1 ($\pi^* \rightarrow \pi^*$) transition, whose beginning is manifested in

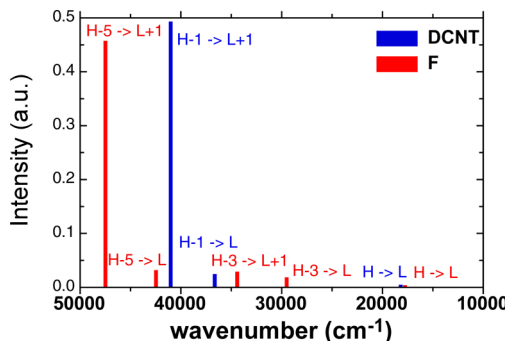
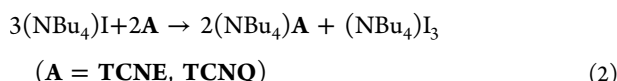


Figure 13. Schematic representations of the UV–vis spectra of DCNT and F (H = HOMO; L = LUMO). See Table 5 for the electronic transitions and their intensities.

the Nujol spectrum (the DMSO spectrum has a solvent cutoff in that region). There is good agreement with the predicted UV–vis spectra for DCNT, TCNE, TCNQ, and TCNP and F (Figure 13 and Table 5).

The similarities in the orbital energies and the shapes of the HOMOs and LUMOs of DCNT and F (Figures 5 and 6) explain the similar positions and intensities of the lowest-energy transition (the HOMO → LUMO transition), which appears at about $17\,000\text{ cm}^{-1}$ in both cases. The similarity between the HOMO–1 orbital of DCNT and the HOMO–5 orbital in F explains the similarity in the highest two transitions. However, between $30\,000$ and $35\,000\text{ cm}^{-1}$ there are two transitions in F that are not present in DCNT that are responsible for the different colors of these two molecules: the HOMO–3 → LUMO and HOMO–3 → LUMO+1 transitions. HOMO–3 has a shape whose dominant component is on the amido groups. In DCNT, the corresponding orbital is placed lower in energy because of the higher electronegativity of the CN groups.

5. Electrochemistry and Reactivity of DCNT. DCNT was reported to have a reversible one-electron reduction potential of 0.09 V vs SCE in MeCN¹² and hence is easier to reduce than TCNE. Both TCNE and TCNQ are reduced by iodides [e.g., $(\text{NBu}_4)\text{I}$] to form $[\text{TCNE}]^{\bullet-}$ and $[\text{TCNQ}]^{\bullet-}$, respectively (eq 2):



However, the reaction of DCNT and $(\text{NBu}_4)\text{I}$ did not lead to tractable products, and decomposition under many reaction conditions was evident.

DCNT was also anticipated to react with $\text{Fe}^{\text{II}}(\text{C}_5\text{Me}_5)_2$ to form the electron transfer salt $[\text{Fe}^{\text{III}}(\text{C}_5\text{Me}_5)_2]^+[\text{DCNT}]^{\bullet-}$, which like $[\text{Fe}^{\text{III}}(\text{C}_5\text{Me}_5)_2]^+[\text{TCNE}]^{\bullet-}$ should exhibit ferromagnetic coupling if not order as a ferromagnet, as occurs for several electron transfer salts of $[\text{Fe}^{\text{III}}(\text{C}_5\text{Me}_5)_2]^+[\text{acceptor}]^{\bullet-}$ composition.³⁸ Upon reaction of $\text{Fe}^{\text{II}}(\text{C}_5\text{Me}_5)_2$ and DCNT in THF, the reaction mixture turned green, suggestive of electron transfer. Moreover, the IR spectrum of the product exhibited a $\nu_{\text{C}\equiv\text{N}}$ absorption at 2222 cm^{-1} , which is 51 cm^{-1} lower than that observed for DCNT⁰, suggesting its reduction. Nonetheless, a pure product could not be isolated. The reaction in MeCN led to products that lacked an absorption in the 2300 – 2000 cm^{-1} region assignable to $\nu_{\text{C}\equiv\text{N}}$. Unlike analogous reactions with either TCNE or TCNQ, only a brown precipitate was formed, which also lacked an absorption assignable to $\nu_{\text{C}\equiv\text{N}}$.

As the failure to form salts of $[\text{DCNT}]^{\bullet-}$ was unexpected, the solution electrochemistry was revisited to verify its solution redox behavior.

The reaction of TCNP and $\text{V}(\text{CO})_6$ forms magnetically ordered $\text{V}[\text{TCNP}]_2\cdot z\text{CH}_2\text{Cl}_2$ with $T_c = 200\text{ K}$.⁸ DCNT, like TCNE, TCNQ, and TCNP, forms an immediate black precipitate upon reaction with $\text{V}(\text{CO})_6$. The product, however, lacks a $\nu_{\text{C}\equiv\text{N}}$ absorption indicative of decomposition. The temperature-dependent magnetic susceptibility [$\chi(T)$] of this product is characteristic of antiferromagnetic coupling (as $\chi(T) \times T$ decreases with decreasing temperature) and lacks evidence of magnetic ordering above 4 K , so this product was not studied further. The decomposition of DCNT was unexpected in view of the report of its reversible one-electron reduction. Hence, decomposition upon reduction with $\text{V}(\text{CO})_6$ does not lead to the formation of a magnetically ordered material.

The electrochemistry of DCNT was also studied by cyclic voltammetry of a 1 mM solution in MeCN (with 0.1 M $[\text{NBu}_4]\text{[PF}_6]$ as the supporting electrolyte). An irreversible one-electron reduction is observed at -0.09 V vs SCE (Figure 14).

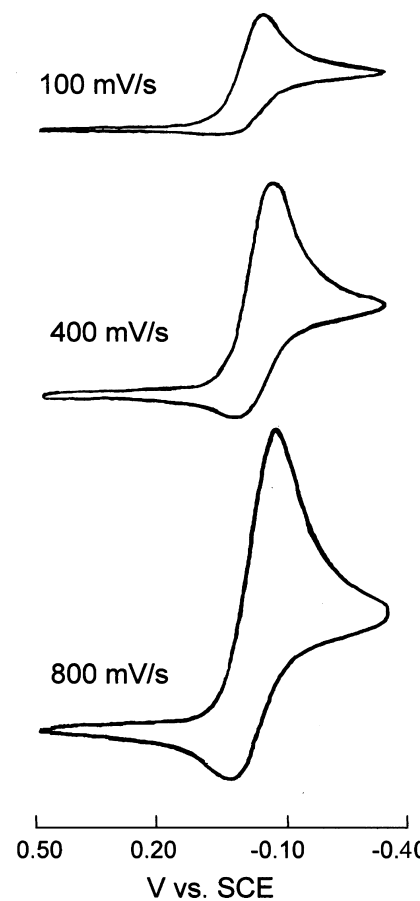
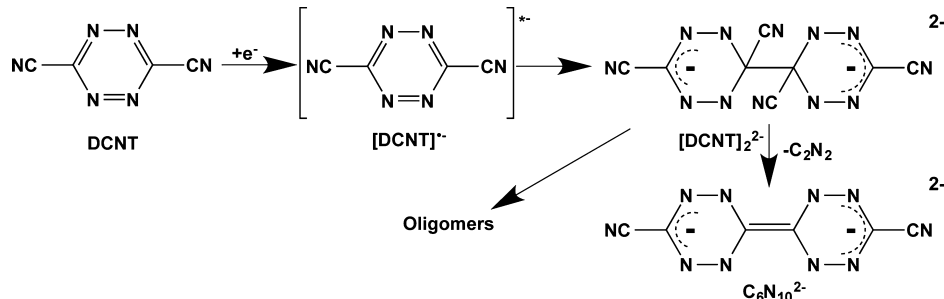


Figure 14. Cyclic voltammograms for DCNT at 100, 400, and 800 mV/s revealing an irreversible one-electron reduction.

This is in contrast with the report of a reversible reduction at 0.09 V vs SCE in MeCN.¹² The irreversible reduction of DCNT is in contrast to the reversible reductions established for TCNE, TCNQ, and TCNP (see Table 4) but comparable to the irreversible behavior reported for tricyanotriazine and 1,3,5-tricyanobenzene.¹⁷

On the basis of the reduction of 1,3,5-tricyanotriazine and 1,3,5-tricyanobenzene¹⁷ and the inability to isolate the sought

Scheme 2. Hypothesized Reduction Pathways for DCNT



$[DCNT]^{•-}$, it is likely that $[DCNT]^{•-}$ dimerizes to form $[DCNT]_2^{•-}$ (Scheme 2), akin to the formation of $[1,3,5\text{-tricyanotriazene}]_2^{2-}$. We further speculate that $[DCNT]_2^{•-}$ could lose cyanogen to form $[C_6N_{10}]^{2-}$, akin to the formation of redox-active $[C_{12}N_{12}]^{2-}$ from $[1,3,5\text{-tricyanotriazene}]_2^{2-}$.¹⁷ However, neither species could be detected or isolated. The inability to characterize any of these reduced DCNT-based species suggests that oligomers of reduced DCNT form.

CONCLUSION

1,4-Dicyanotetrazine (DCNT) was prepared by a modified literature procedure.⁴⁰ From electrochemical studies, DCNT exhibits an irreversible one-electron reduction at -0.09 V vs SCE in MeCN and is a little harder to reduce than TCNQ and TCNE but easier to reduce than TCNP. However, the irreversible reduction suggests that the putative radical anion, $[DCNT]^{•-}$, is reactive and to likely form dimers if not oligomers, as observed for 1,3,5-tricyanotriazene and 1,3,5-tricyanobenzene.¹⁷ The precursor to DCNT, 1,2,4,5-tetrazine-3,6-dicarboxamide (F), exhibits an usual deep-magenta color in the solid state. Its hydrogen-bonded layered structure was determined, and it was found to exhibit bands at $37\,000\text{ cm}^{-1}$ (270 nm) and $18\,500\text{ cm}^{-1}$ (541 nm) that are assigned to HOMO-5 \rightarrow LUMO and HOMO \rightarrow LUMO transitions, respectively. It has a broad absorption band starting at $18\,800\text{ cm}^{-1}$, giving rise to the magenta color of the powder, and chromaticity coordinates of $x = 0.42$ and $y = 0.31$, corresponding to the pink/red/orange region on the 1931 CIE chromaticity diagram.

EXPERIMENTAL SECTION

Materials. All of the syntheses were performed under a dry N_2 atmosphere in a glovebox (<1 ppm O_2). Acetonitrile was purified through an activated alumina dual-column purification system under a positive pressure of dry N_2 . Diethyl ether (Et_2O), acetone (Me_2CO), and tetrahydrofuran (THF) were purified via distillation under dry N_2 . Glycine ethyl ester hydrochloride and tetrakis(dimethylamino)-ethylene (TDAE) were purchased and used without further purification. $V(CO)_6$ was prepared from $[NEt_4][V(CO)_6]$ and phosphoric acid and purified by sublimation at 25 °C and 0.05 Torr.³⁹ Ferrocene was sublimed prior to use. Nitrous gas was formed *in situ* by the reaction of hydrochloric acid with sodium nitrite.⁴⁰

Synthesis of DCNT. DCNT can be prepared by a published procedure;¹¹ however, it was synthesized via a modified and extended version of the method from the literature, starting from commercially available ethyl diazoacetate (Scheme 1).⁴⁰ A solution of sodium hydroxide (160 g, 4 mol) in 250 mL of water was stirred at 60 °C while ethyl diazoacetate (100 g, 875 mmol) (A) was added dropwise. After ~ 1 h, the reaction slurry was cooled to room temperature and was washed with 1 L of 95% ethanol five times. The precipitate was collected by filtration, washed sequentially with 500 mL of absolute ethanol and 500 mL of anhydrous ether, and dried in air to give

disodium dihydro-1,2,4,5-tetrazine-3,6-dicarboxylate (B) as a yellow-brown solid (83 g, 88%).

A solution of B (75 g, 0.35 mol) in 85 mL of water and crushed ice (83 g) was cooled by a sodium chloride bath while a solution of concentrated hydrochloric acid (36–38%, 70 mL) was added dropwise with stirring. The reaction mixture was washed five times with anhydrous ether, filtered, and dried under reduced pressure to give yellow/orange dihydro-1,2,4,5-tetrazine-3,6-dicarboxylic acid (C) (41 g, 69%).

Thionyl chloride (32 mL, 0.466 mol) was slowly added to a stirring -30 °C cooled solution of absolute methanol (600 mL). Compound C (38 g, 221 mol) was added to the cooled solution in small portions over 30 min. The reaction mixture was then warmed to room temperature and subsequently warmed to 35 °C for 2 h. The reaction mixture was cooled, and the precipitate was collected by filtration. The solid was washed with ether and triturated with dichloromethane, while the filtrate was concentrated to give an orange-brown oil that was extracted with dichloromethane six times. The combined dichloromethane extracts and trituration were dried with magnesium sulfate and concentrated to give yellow/orange dimethyl dihydro-1,2,4,5-tetrazine-3,6-dicarboxylate (D) (20 g, 45%).

Compound D (17 g, 85 mmol) was dissolved in concentrated ammonium hydroxide (200 mL) containing 1.70 g of ammonium chloride. The mixture was stirred at room temperature for 12 h. The resulting product was filtered and washed with water and ethanol to give dihydro-1,2,4,5-tetrazine-3,6-dicarboxamide (E) as a yellow solid (14.1 g, 98%).

Compound E (7 g, 41 mmol) was added to 500 mL of water, and the mixture was chilled to 0 °C to give a yellow slurry. A stream of nitrous oxide gas was bubbled directly into the reaction mixture producing a color change from yellow to hot pink. The reaction mixture was filtered and dried to afford magenta 1,2,4,5-tetrazine-3,6-dicarboxamide (F) (5.68 g, 82%). F has poor solubility except in DMSO and DMF. UV-vis (DMSO) $\lambda_{max}/\text{cm}^{-1}$: 38 800 (258 nm; $\epsilon = 7500\text{ cm}^{-1}\text{ M}^{-1}$), 19 200 (520 nm; $\epsilon = 840\text{ cm}^{-1}\text{ M}^{-1}$); UV-vis (Nujol) $\lambda_{max}/\text{cm}^{-1}$: 37 000 (270 nm), 18 500 (541 nm).

Diamide F (1 g, 6 mmol) was finely ground in a mortar and pestle with P_2O_5 (5 g, 35 mmol), and the mixture was heated at 160 °C in vacuo in a sublimation apparatus at 10^{-4} Torr via an oil diffusion pump. The sublimed product was further purified by an additional sublimation in vacuo at 60 °C to give pure 1,4-dicyanotetrazine (DCNT) as orange-red crystals (100 mg, 10%). IR (cm^{-1}): 2271 (m, $\nu_{C\equiv N}$), 1345 (s), 1281 (w), 904 (m), 850 (m), 810 (w), 588 (s), 515 (m). UV-vis (MeCN) $\lambda_{max}/\text{cm}^{-1}$: 45 000 (222 nm; $\epsilon = 57\,000\text{ cm}^{-1}\text{ M}^{-1}$), 36 600 (273 nm; $\epsilon = 17\,400\text{ cm}^{-1}\text{ M}^{-1}$), 20 400 (491 nm; $\epsilon = 2500\text{ cm}^{-1}\text{ M}^{-1}$).

Physical Methods. *Crystal Structure Determination.* An orange prism of DCNT was selected, mounted on a thin glass fiber using a viscous oil, and then transferred to a diffractometer equipped with Mo $K\alpha$ radiation. Ten frames of data were collected with an oscillation range of $1^\circ/\text{frame}$ and an exposure time of 20 s/frame.^{41a} A total of 613 reflections were indexed, integrated, and corrected for Lorentz, polarization, and absorption effects using DENZO-SMN and SCALEPAC.^{41b} Crystallographic information is summarized in Table 1. The structure was solved using direct methods, and heavy atoms were

solved using SIR97.^{41c} All of the non-hydrogen atoms were refined with anisotropic displacement coefficients. The weighting scheme employed was $w = 1/[\sigma^2(F_o^2) + (0.0379P)^2 + 0.2385P]$, where $P = (F_o^2 + 2F_c^2)/3$. All of the software and sources of scattering factors are contained in the SHELXTL program library.^{41d}

High-resolution powder X-ray diffraction measurements for structural analysis of 1,2,4,5-tetrazine-3,6-dicarboxamide were performed at beamline X16C at the National Synchrotron Light Source at Brookhaven National Laboratory. The powdered samples were sealed in nominal 1.0 mm diameter thin-wall glass capillaries. X-rays were selected by a channel-cut Si(111) monochromator. Diffracted X-rays were selected by a Ge(111) analyzer and detected by a NaI scintillation counter. The capillary was spun at several hertz during data collection to improve the particle statistics. The incident intensity was monitored by an ion chamber and used to normalize the measured signal. TOPAS-Academic was used to index, solve, and refine the crystal structures.^{42,43}

Spectroscopic Studies. Infrared spectra were taken from 400 to 4000 cm^{-1} using an FTIR spectrometer ($\pm 1 \text{ cm}^{-1}$). Samples were prepared as KBr pellets under an inert atmosphere. UV-vis spectroscopy was carried out on a double-beam, double-monochromator UV-vis-near-IR spectrometer scanning from 190 to 820 nm. Samples were prepared as 0.1 M solutions in MeCN in 1 cm quartz cuvettes. A 60 mm standard integrating sphere diffuse-reflectivity attachment using an optical-grade BaSO₄ white standard was used for the reflectivity studies. Instrument software was employed to convert the diffuse-reflectance spectra into absorbance spectra using a Kubelka-Munk algorithm.⁴⁴

Magnetic Studies. Magnetic susceptibility measurements were made between 5 and 300 K using a SQUID magnetometer equipped with a reciprocating sample measurement system or using a susceptometer equipped with a reciprocating sample measurement system as described previously.⁴⁵ Measurements were made on powders contained in airtight Delrin holders packed with quartz wool to prevent sample movement in the holder. The samples were placed in the magnetometer, and the magnetic field was removed by oscillating the field until it had reached zero. The magnetometer was then cooled, and the field was applied; the data were recorded upon warming. Magnetic studies were conducted in a gelatin capsule. AC susceptibilities were recorded at 33, 100, and 1000 Hz. In addition to correcting for the diamagnetic contribution from the sample holder, the core diamagnetic corrections of -57 and -230×10^{-6} emu/mol were used for DCNT and Fe^{II}(C₅Me₅)₂, respectively.

Electrochemical Studies. Reduction potentials were measured from cyclic voltammograms (CVs) scanning between zero and -0.75 V at scan rates ranging from 100 to 800 mV/s. The reported CVs at 100 mV/s used Pt working and counter electrodes and a Ag/AgNO₃ reference electrode with 0.10 M [NBu₄][PF₆] as the supporting electrolyte in acetonitrile; ferrocene was used as the reference. Reduction potentials are reported in volts vs SCE.

Thermal Studies. Thermogravimetric analysis was conducted in a Vacuum Atmospheres DriLab instrument under an inert atmosphere (N₂) to avoid O₂/H₂O degradation of the samples. Samples were loaded in an aluminum pan and heated for 10 min at 20 °C before the temperature was ramped from 20 to 600 °C at 5.00 °C/min under a continuous 10 mL/min N₂ purge.

Computational Studies. All of the DFT calculations were carried out using the hybrid B3LYP exchange-correlation⁴⁶ density functional and the 6-31++g(d,p) basis set.⁴⁷ The key properties of the electronic structures of DCNT and [DCNT]^{•-} (i.e., MO diagrams, spin densities, charge distributions, and electron affinities) were evaluated at their isolated minimum-energy structures. Frequencies were computed for each optimized structure in order to confirm its true character as a minimum-energy structure. The optimized geometry of DCNT was based upon its crystal structure, while that for [DCNT]^{•-} was computed starting from the structure of its neutral parent DCNT. A similar approach was used for TCNE,⁴⁸ TCNQ,^{49,50} and TCNP,⁵¹ for which the geometries of the corresponding radical anions were optimized starting from the geometries of the parent neutral molecules, and the results were compared against the crystallographic

structures in one of their salts. Table S1 in the Supporting Information contains the main parameters for the optimized geometry of each computed system. The charge distributions were investigated by Mulliken population analysis⁵² and NBO analysis⁵³ and by plotting the MEP maps⁵⁴ of the molecules. The evaluation of the electron affinity (EA), defined as the total energy of the neutral parent molecule minus that for the anion,⁵⁵ was computed for each isolated system as well as in MeCN or CH₂Cl₂ solution. In the last two cases, the energies of the dissolved systems were estimated using the polarized continuum model (PCM),⁵⁶ a type of continuous solvation model in which solvation is described by a series of multipole moments placed around a solute molecule and estimated iteratively using the quantum-mechanical method of choice, here at the B3LYP/6-31++g(d,p) level. It should be noted that the EA in solution is generally measured in terms of the reduction half-wave potential, a closely related electrochemical property whose connection with EA has been studied in the literature.⁵⁷ The optimum geometries of all systems investigated in this work agreed very well with those found in their crystals. The theoretical UV-vis spectra were computed by running TD-DFT calculations using the B3LYP functional and the 6-31++G(d,p) basis set.⁵⁸ All of the calculations were done using Gaussian 09.⁵⁹

ASSOCIATED CONTENT

Supporting Information

Optimum geometries and total energies of the neutral and anionic species and X-ray CIF files for DCNT and F. This material is available free of charge via the Internet at <http://pubs.acs.org>. The crystallographic data have also been deposited with the Cambridge Crystallographic Data Center (<http://www.ccdc.cam.ac.uk>) with reference numbers CCDC 1000683 and 999655, respectively.

AUTHOR INFORMATION

Corresponding Authors

*E-mail: juan.novoa@ub.edu.
*E-mail: jsmiller@chem.utah.edu.

Present Address

[†]S.H.L.: X-ray Science Division, Argonne National Laboratory, Argonne, IL, USA.

Author Contributions

The synthesis and the spectroscopic and magnetic characterizations were done by H.-L.V. and J.S.M, the diffuse-reflectivity and chromaticity analyses by R.K.N. and M.H.B., and the single-crystal X-ray analyses by A.M.A., all at the University of Utah. The PXRD studies were done by S.H.L. and P.W.S. at Brookhaven National Laboratory and Stony Brook University. The computational analyses were executed by M.C.-C. and J.J.N. at the Universitat de Barcelona.

Notes

The authors declare no competing financial interest.

ACKNOWLEDGMENTS

We thank Drs. Trent D. Selby, William W. Shum, and Michelle L. Taliaferro for providing preliminary data and the Department of Energy, Division of Materials Science (Grant DE-FG03-93ER45504) for support. Use of the National Synchrotron Light Source at Brookhaven National Laboratory was supported by the U.S. Department of Energy, Office of Basic Energy Sciences, under Contract DE-AC02-98CH10886. R.K.N. and M.H.B. acknowledge support by the Research Corporation for Science Advancement (Scialog Program). Computational work at the University of Barcelona was supported by the Spanish MINECO (MAT2011-25972) and the Catalan Autonomous Government (2009-SGR-1203), and

the computer time was provided by CESCA and BSC. We thank Eric V. Campbell and Andrew N. Simonson for acquiring the electronic absorption spectrum of TCNP and the diffuse-reflectivity spectrum of F.

■ REFERENCES

- (1) Reviews: (a) Ocharenko, V. I.; Sagdeev, R. Z. *Russ. Chem. Rev.* **1999**, *68*, 45. (b) Miller, J. S.; Epstein, A. J. *Angew. Chem., Int. Ed. Engl.* **1994**, *33*, 385. (c) Kinoshita, M. *Jpn. J. Appl. Phys.* **1994**, *33*, 5718. (d) Caneschi, A.; Gatteschi, D. *Prog. Inorg. Chem.* **1991**, *37*, 331. (e) Crayson, J. A.; Devine, J. N.; Walton, J. C. *Tetrahedron* **2000**, *56*, 7829. (f) Blundell, S. J.; Pratt, F. L. *J. Phys.: Condens. Matter* **2004**, *16*, R771.
- (2) Conference proceedings: (a) Day, P.; Underhill, A. E. Metal–Organic and Organic Molecular Magnets. *Philos. Trans. R. Soc. London, Ser. A* **1999**, *357*, 2849. (b) *Proceedings of the 6th International Conference on Molecule-Based Materials*; Kahn, O., Ed.; *Molecular Crystals and Liquid Crystals*, Vol. 334/335, 1999. (c) *Proceedings of the 7th International Conference on Molecule-Based Magnets*; Christou, G., Ed.; *Polyhedron*, Vol. 20, 2001. (d) *Proceedings of the 8th International Conference on Molecule-Based Magnets*; Christou, G., Ed.; *Polyhedron*, Vol. 22, Issues 14–17, 2003.
- (3) Miller, J. S.; Calabrese, J. C.; Epstein, A. J.; Bigelow, R. W.; Zhang, J. H.; Reiff, W. M. *J. Chem. Soc., Chem. Commun.* **1986**, 1026.
- (4) Miller, J. S. *J. Mater. Chem.* **2010**, *20*, 1846.
- (5) Manriquez, J. M.; Yee, G. T.; McLean, R. S.; Epstein, A. J.; Miller, J. S. *Science* **1991**, *252*, 1415.
- (6) Zhang, J.; Zhou, P.; Brinckerhoff, W. B.; Epstein, A. J.; Vazquez, C.; McLean, R. S.; Miller, J. S. *ACS Symp. Ser.* **1996**, *644*, 311.
- (7) Vickers, E. B.; Selby, T. D.; Thorum, M. S.; Taliaferro, M. L.; Miller, J. S. *Inorg. Chem.* **2004**, *43*, 6414.
- (8) Vickers, E. B.; Selby, T. D.; Miller, J. S. *J. Am. Chem. Soc.* **2004**, *126*, 3716.
- (9) Taliaferro, M. L.; Thorum, M. S.; Miller, J. S. *Angew. Chem., Int. Ed.* **2006**, *45*, 5326.
- (10) Hamlin, J. J.; Beckett, B. R.; Tomita, T.; Schilling, J. S.; Tyree, W. S.; Yee, G. T. *Polyhedron* **2003**, *22*, 2249.
- (11) (a) Berlin, A.; Pagni, G. A.; Sannicolo, F. *J. Chem. Soc., Chem. Commun.* **1986**, 1579. (b) Berlin, A.; Pagni, G. A.; Sannicolo, F. *Synth. Met.* **1987**, *19*, 415.
- (12) Gleiter, R.; Schehlmann, V.; Spanget-Larsen, J.; Fischer, H.; Neugebauer, F. A. *J. Org. Chem.* **1988**, *53*, 5756.
- (13) Moscherosch, M.; Waldhöer, E.; Binder, H.; Kaim, W.; Fiedler, J. *J. Inorg. Chem.* **1995**, *34*, 4326.
- (14) Bond, A. M.; Cotton, F. A. *Inorg. Chem.* **1976**, *15*, 2036.
- (15) Subrayan, R. P.; Rasmussen, P. G. *Trends Polym. Sci.* **1995**, *3*, 165.
- (16) Hill, M.; Mahon, M. F.; Molloy, K. C. *J. Chem. Soc., Dalton Trans.* **1996**, 1857.
- (17) Del Sesto, R. E.; Arif, A. M.; Novoa, J. J.; Anusiewicz, I.; Skurski, P.; Simons, J.; Dunn, B. C.; Eyring, E. M.; Miller, J. S. *J. Org. Chem.* **2003**, *68*, 3367.
- (18) Brandon, E. J.; Burkhardt, B. M.; Rogers, R. D.; Miller, J. S. *Chem.—Eur. J.* **1998**, *4*, 1938.
- (19) (a) Gillan, E. G. *Chem. Mater.* **2000**, *12*, 3906. (b) Kapotke, T.; Kuffer, C.; Mayer, P.; Polborn, K.; Schulz, A.; Weigand, J. J. *Inorg. Chem.* **2005**, *44*, 5949. (c) Wei, T.; Zhu, W.; Zhang, X.; Li, Y.-F.; Xiao, H. *J. Phys. Chem. A* **2009**, *113*, 9404.
- (20) Kaim, W. *Coord. Chem. Rev.* **2002**, *230*, 127.
- (21) As in Ne···Ne and other noble gas dimers, where no attractive electrostatic component exists between the fragments and no hydrogen bond is present, the dominant attractive component originates only in the dispersion (i.e., van der Waals) interactions among the paired electrons. Dispersion is particularly important when the number of lone-pair electrons overlapping with the orbitals where they are contained is large, as in Ne···Ne, halogen···halogen, or π ··· π interactions. Dispersion also increases when the number of overlapping lone-pair electrons increases, i.e., He···He < Ne···Ne < Ar···Ar < Kr···Kr.
- (22) Allen, H. F.; Motherwell, D. W. S.; Raithby, R. P.; Shields, P. G.; Taylor, R. *New J. Chem.* **1999**, *23*, 25.
- (23) (a) Jurečka, P.; Šponer, J.; Černý, J.; Hobza, P. *Phys. Chem. Chem. Phys.* **2006**, *8*, 1985. (b) Lee, E. C.; Kim, D.; Jurečka, P.; Tarakeshwar, P.; Hobza, P.; Kim, K. S. *J. Chem. Phys. A* **2007**, *111*, 3446.
- (24) Del Sesto, R. E.; Miller, J. S.; Lafuente, P.; Novoa, J. J. *J. Chem.—Eur. J.* **2002**, *8*, 4894.
- (25) Milián, B.; Pou-Amérigo, R.; Viruela, R.; Ortí, E. *Chem. Phys. Lett.* **2003**, *375*, 376.
- (26) Capdevila-Cortada, M.; Novoa, J. J.; Bell, J. D.; Moore, C. E.; Rheingold, A. L.; Miller, J. S. *Chem.—Eur. J.* **2011**, *17*, 9326.
- (27) Garcia-Yoldi, I.; Miller, J. S.; Novoa, J. J. *J. Phys. Chem. A* **2009**, *113*, 7124.
- (28) Milián, B.; Pou-Amérigo, R.; Viruela, R.; Ortí, E. *Chem. Phys. Lett.* **2004**, *391*, 148.
- (29) Novoa, J. J.; Stephens, P. W.; Weerasakare, M.; Shum, W. W.; Miller, J. S. *J. Am. Chem. Soc.* **2009**, *131*, 9070.
- (30) (a) Szabo, A.; Ostlund, N. S. *Modern Quantum Chemistry: Introduction to Advanced Electronic Structure Theory*; 1st rev. ed.; McGraw-Hill: New York, 1989. (b) Novoa, J. J.; Deumal, M.; Jornet-Somoza, J. *Chem. Soc. Rev.* **2011**, *40*, 3182.
- (31) (a) Novoa, J. J.; Rovira, M. C.; Rovira, C.; Veciana, J.; Tarres, J. *Adv. Mater.* **1995**, *7*, 233. (b) Braga, D.; Bazzi, C.; Grepioni, F.; Novoa, J. J. *New J. Chem.* **1999**, *23*, 577.
- (32) Rienstra-Kiracofe, J. C.; Tschumper, G. S.; Schaefer, H. F., III; Nandi, S.; Ellison, G. B. *Chem. Rev.* **2002**, *102*, 231.
- (33) (a) Peover, M. E. *Nature* **1962**, *193*, 475. (b) Elkechai, A.; Boucekkine, A.; Belkhiri, L.; Amarouche, M.; Clappe, C.; Hauchard, D.; Ephritikhine, M. *Dalton Trans.* **2009**, 2843.
- (34) Chen, E. C. M.; Wentworth, W. E. *J. Chem. Phys.* **1975**, *63*, 3183.
- (35) Audebert, P.; Sadki, S.; Miomandre, F.; Clavier, G. *Electrochem. Commun.* **2004**, *6*, 144–147.
- (36) (a) Wyszecki, G.; Stiles, W. S. *Color Science: Concepts and Methods, Quantitative Data and Formulae*; Wiley: New York, 1982. (b) Srinivasarao, M. *Chem. Rev.* **1999**, *99*, 1935.
- (37) (a) Kaiser, P. K.; Boynton, R. M. *Human Color Vision*; Optical Society of America: Washington, DC, 1996. (b) Foster, D. H. *Vision Res.* **2011**, *51*, 674.
- (38) Yee, G. T.; Miller, J. S. In *Magnetism—Molecules to Materials*; Miller, J. S., Drillon, M., Eds.; Wiley-VCH: Weinheim, Germany, 2004; Vol. 5, p 223.
- (39) Liu, X.; Ellis, J. E.; Selby, T. D.; Ghalsasi, P.; Miller, J. S. *Inorg. Synth.* **2004**, *34*, 68.
- (40) Boger, D. L.; Coleman, R. S.; Panek, J. S.; Huber, F. X.; Sauer, J. *J. Org. Chem.* **1985**, *50*, 5377.
- (41) (a) COLLECT Data Collection Software; Nonius B.V.: Delft, The Netherlands, 1998. (b) Otwinski, Z.; Minor, W. *Methods Enzymol.* **1997**, *276*, 307. (c) Altomare, A.; Burla, M. C.; Camalli, M.; Cascarano, G.; Giacovazzo, C.; Guagliardi, A.; Moliteni, G. G.; Polidori, G.; Spagna, R. *SIR97—A Program for Automatic Solution and Refinement of Crystal Structure*, release 1.02. (d) Sheldrick, G. M. *SHELX97: Programs for Crystal Structure Analysis* (includes SHELXS97, SHELXL97, CIFTAB); release 97-2, University of Göttingen: Göttingen, Germany, 1997; version 5.10, Bruker AXS: Madison, WI, 1998.
- (42) Coelho, A. A. *TOPAS Academic Version 4.1 Technical Reference*; Coelho Software: Brisbane, Australia, 2007; software and documentation available at www.topas-academic.net.
- (43) Coelho, A. A. *J. Appl. Crystallogr.* **2000**, *33*, 899.
- (44) Torrent, J.; Barrón, V. *Encyclopedia of Surface and Colloid Science*; Marcel Dekker: New York, 2002.
- (45) Brandon, E. J.; Rittenberg, D. K.; Arif, A. M.; Miller, J. S. *Inorg. Chem.* **1998**, *37*, 3376.
- (46) The B3LYP hybrid functional is a combination of Becke's nonlocal three-parameter exchange functional and the Lee–Yang–Parr

- nonlocal correlation functional. See: Becke, A. D. *J. Chem. Phys.* **1993**, 98, S648. Lee, C.; Yang, W.; Parr, R. G. *Phys. Rev. B* **1998**, 37, 785.
- (47) (a) Ditchfield, R.; Hehre, W. J.; Pople, J. A. *J. Chem. Phys.* **1971**, 54, 724. (b) Clark, T.; Chandrasekhar, J.; Spitznagel, G. W.; Schleyer, P. v. R. *J. Comput. Chem.* **1983**, 4, 294.
- (48) Chaplot, S. L.; Mierzejewski, A.; Pawley, G. S. *Acta Crystallogr.* **1984**, C40, 663.
- (49) Long, R. E.; Sparks, R. A.; Trueblood, K. N. *Acta Crystallogr.* **1965**, 18, 932.
- (50) Schultz, A. J.; Stucky, G. D.; Blessing, R. H.; Coppens, P. *J. Am. Chem. Soc.* **1976**, 98, 3194.
- (51) Rosokha, S. V.; Liu, J.; Han, B.; Kochi, J. K. *New J. Chem.* **2009**, 33, 545.
- (52) Mulliken, R. S. *J. Chem. Phys.* **1955**, 23, 1833.
- (53) Reed, A. E.; Curtiss, L. A.; Weinhold, F. *Chem. Rev.* **1988**, 88, 899.
- (54) Tomasi, J.; Mennucci, B.; Cammi, R. *Theor. Comput. Chem.* **1996**, 3, 1.
- (55) Muller, P. *Pure Appl. Chem.* **1994**, 66, 1077.
- (56) Tomasi, J.; Mennucci, B.; Cammi, R. *Chem. Rev.* **2005**, 105, 2999.
- (57) (a) Pearson, R. G. *J. Am. Chem. Soc.* **1986**, 108, 6109. (b) Ruoff, R. S.; Kadish, K. M.; Boulas, P.; Chen, E. C. M. *J. Phys. Chem.* **1995**, 99, 8843.
- (58) (a) Stratmann, R. E.; Scuseria, G. E.; Frisch, M. J. *J. Chem. Phys.* **1998**, 109, 8218. (b) Bauernschmitt, P.; Ahlrichs, R. *Chem. Phys. Lett.* **1996**, 256, 454. (c) Casida, M. E.; Jamorski, C.; Casida, K. C.; Salahub, D. R. *J. Chem. Phys.* **1998**, 108, 4439.
- (59) Frisch, M. J.; Trucks, G. W.; Schlegel, H. B.; Scuseria, G. E.; Robb, M. A.; Cheeseman, J. R.; Scalmani, G.; Barone, V.; Mennucci, B.; Petersson, G. A.; Nakatsuji, H.; Caricato, M.; Li, X.; Hratchian, H. P.; Izmaylov, A. F.; Bloino, J.; Zheng, G.; Sonnenberg, J. L.; Hada, M.; Ehara, M.; Toyota, K.; Fukuda, R.; Hasegawa, J.; Ishida, M.; Nakajima, T.; Honda, Y.; Kitao, O.; Nakai, H.; Vreven, T.; Montgomery, J. A., Jr.; Peralta, J. E.; Ogliaro, F.; Bearpark, M.; Heyd, J. J.; Brothers, E.; Kudin, K. N.; Staroverov, V. N.; Kobayashi, R.; Normand, J.; Raghavachari, K.; Rendell, A.; Burant, J. C.; Iyengar, S. S.; Tomasi, J.; Cossi, M.; Rega, N.; Millam, N. J.; Klene, M.; Knox, J. E.; Cross, J. B.; Bakken, V.; Adamo, C.; Jaramillo, J.; Gomperts, R.; Stratmann, R. E.; Yazyev, O.; Austin, A. J.; Cammi, R.; Pomelli, C.; Ochterski, J. W.; Martin, R. L.; Morokuma, K.; Zakrzewski, V. G.; Voth, G. A.; Salvador, P.; Dannenberg, J. J.; Dapprich, S.; Daniels, A. D.; Farkas, Ö.; Foresman, J. B.; Ortiz, J. V.; Cioslowski, J.; Fox, D. J. *Gaussian 09*, revision D.01; Gaussian, Inc.: Wallingford, CT, 2009.
- (60) Montalti, M.; Credi, A.; Luca, P.; Gandolfi, M. *Handbook of Photochemistry*, 3rd ed.; CRC Press: Boca Raton, FL, 2006; p 493.
- (61) Chowdhury, S.; Kebarle, P. *J. Am. Chem. Soc.* **1986**, 108, 5453.
- (62) Compton, R. N.; Cooper, C. D. *J. Chem. Phys.* **1977**, 66, 4325.
- (63) Kanai, K.; Akaike, K.; Koyasu, K.; Sakai, K.; Nishi, T.; Kamizuru, Y.; Nishi, T.; Ouchi, Y.; Seki, K. *Appl. Phys. A: Mater. Sci. Process.* **2009**, 95, 309.
- (64) Dixon, D. A.; Miller, J. S. *J. Am. Chem. Soc.* **1987**, 109, 3656.
- (65) Hiroma, S.; Koruda, H.; Akamatu, H. *Bull. Chem. Soc. Jpn.* **1970**, 43, 3626.